WATER RESOURCES RESEARCH, VOL. 49, 6179–6193, doi:10.1002/wrcr.20448, 2013

A nonparametric stochastic method for generating daily climate-adjusted streamflows

J. H. Stagge[1] and G. E. Moglen[1]

Received 30 July 2012; revised 21 July 2013; accepted 26 July 2013; published 2 October 2013.

[1] A daily stochastic streamflow generation model is presented, which successfully replicates statistics of the historical streamflow record and can produce climate-adjusted daily time series. A monthly climate model relates general circulation model (GCM)-scale climate indicators to discrete climate-streamflow states, which in turn control parameters in a daily streamflow generation model. Daily flow is generated by a two-state (increasing/decreasing) Markov chain, with rising limb increments randomly sampled from a Weibull distribution and the falling limb modeled as exponential recession. When applied to the Potomac River, a 38,000 km^2 basin in the Mid-Atlantic United States, the model reproduces the daily, monthly, and annual distribution and dynamics of the historical streamflow record, including extreme low flows. This method can be used as part of water resources planning, vulnerability, and adaptation studies and offers the advantage of a parsimonious model, requiring only a sufficiently long historical streamflow record and large-scale climate data. Simulation of Potomac streamflows subject to the Special Report on Emissions Scenarios (SRES) A1b, A2, and B1 emission scenarios predict a slight increase in mean annual flows over the next century, with the majority of this increase occurring during the winter and early spring. Conversely, mean summer flows are projected to decrease due to climate change, caused by a shift to shorter, more sporadic rain events. Date of the minimum annual flow is projected to shift 2–5 days earlier by the 2070–2099 period.

Citation: Stagge, J. H., and G. E. Moglen (2013), A nonparametric stochastic method for generating daily climate-adjusted streamflows, *Water Resour. Res.*, *49*, 6179–6193, doi:10.1002/wrcr.20448.

1. Introduction

[2] Water resources planners and engineers are currently attempting to reconcile two competing concepts: that water management policy must adapt to address the nonstationary nature of hydrologic systems and that estimates of streamflow effects due to climate change often have greater uncertainty than climatic variables, such as temperature, precipitation, and evapotranspiration [*Matalas*, 1997]. As stated by *Srikanthan and McMahon* [2001], one of the major gaps in the design and operation of hydrological systems is the quantification of uncertainty as a result of climatic variability.

[3] This paper presents a novel extension of existing daily stochastic streamflow models [*Sargent*, 1979; *Aksoy and Bayazit*, 2000; *Szilagyi et al*., 2006] to generate an infinite set of long climate-adjusted streamflow time series. This is accomplished by linking parameters of a daily streamflow generation model to discrete climate-streamflow states in a monthly Markov-chain climate model. Climate-streamflow states are classified using historical general circulation model (GCM)-scale climate indicators and state transition probabilities are modified to simulate nonstationarity.

[4] The method is designed as a means to extend the historical record and expand the set of feasible streamflow time series for use in water resources planning, vulnerability, and adaptation studies. This procedure uses a physically based statistical model to generate streamflow traces that reproduce historical flow distributions at multiple temporal scales (daily, monthly, and annual), while also reproducing watershed dynamics, including extreme low flows, hydrograph shape, and serial correlation. Parameters are linked to climate predictors so that the effects of climate change on daily streamflow may be simulated using watershed response to historical climatic variability.

[5] The model was originally developed to generate long sequences of feasible streamflow time series in the Potomac River to simulate, analyze, and optimize water management policies. The 38,000 km^2 Potomac River basin is located in the Mid-Atlantic United States, along the borders of Maryland, Virginia, and West Virginia. The Potomac River is vital for supplying water to the Washington, D. C., metropolitan area, accounting for approximately 78% of the region's annual water demand [*Ahmed et al*., 2010]. In light of this importance, a quantitative evaluation of the effects of climate change on the Potomac River was needed

[1]Department of Civil and Environmental Engineering, Virginia Tech, Falls Church, Virginia, USA.

Corresponding author: J. H. Stagge, Department of Civil and Environmental Engineering, Virginia Tech, 7054 Haycock Road, Falls Church, VA 22043, USA. (jhstagge@vt.edu)

0043-1397/13/10.1002/wrcr.20448

to ensure that water management plans are sufficiently robust to satisfy future requirements.

[6] Attempts to use the existing HSPF-based Chesapeake Bay Watershed Phase 5.3 Model [*U.S. Environmental Protection Agency*, 2010] for this purpose produced unrealistically low drought flows in the Potomac River, prompting attempts to develop alternative means to reproduce streamflow dynamics and statistics. At the Little Falls Station (USGS gauge 01646500), used as a case study herein, the Chesapeake Bay Model underpredicts the annual 7 day low flow during each year of its calibration period 1984–2005, with a mean bias of 2.26×10^6 m^3/day, or 57.1%, and produces only a moderate Nash-Sutcliffe efficiency of 0.508 when viewed on a continuous, daily basis. Errors in modeled low flows are likely related to an emphasis during model development by the EPA on pollutant fluxes, which depend more highly on typical and high flows. While not as physically comprehensive as a rainfall-runoff model such as the Chesapeake Bay Model, the proposed method is more capable of generating random streamflow time series that reproduce the historical distribution and dynamics of the Potomac River, while also allowing for relatively simple evaluation of climate change scenarios in the region.

[7] This paper first presents the analysis and streamflow generation procedure of the proposed method in detail. This method is an extensible framework, which can be expanded and modified to meet particular modeling needs. Details of the Potomac River basin case study are then presented. The model and its application in the Potomac River are validated by generating streamflow traces that reproduce the distribution of the historical streamflow record. The model is further tested using GCM simulations of the 20th century to determine which GCMs perform best and if there are consistent biases among the GCM results. Finally, climate change scenarios are simulated using the developed models and compared to other projections of climate change effects on the region's water resources.

2. Background

2.1. Stochastic Streamflow Models

[8] Stochastic streamflow methods originally focused on long-term water planning and tended to operate at the monthly or annual time scale, typically employing some form of the autoregressive (AR) model. One of the first autoregressive models used for streamflow generation, the Thomas-Fiering model [*Thomas and Fiering*, 1962] is, in essence, a periodic lag-one AR(1) process. Though still employed, the Thomas-Fiering model has generally been supplanted by the Box-Jenkins set of autoregressive-moving average (ARMA) functional forms [*Box and Jenkins*, 1970]. ARMA(1,1) models have generally been shown to be more effective at generating monthly streamflow time series [*Bartolini and Salas*, 1993; *Stedinger et al*., 1985]. These models are sometimes classified as periodic autoregressive moving average (PARMA) models, referring to their periodic structure, with seasonally varying means, standard deviations, and lag coefficients.

[9] In their most basic form, autoregressive models assume normality, which is rare in natural streams. Flows tend to be positively skewed, with a lower bound related to baseflow, and an unbounded upper tail, corresponding to extreme flood events. To effectively use autoregressive models, raw flows must be transformed to approximate a normal distribution, using several available methods including differencing, logarithm transforms, the gamma distribution [*Hirsch*, 1979], or the Box-Cox transformation [*Box and Cox*, 1964]. Without these transformations, autoregressive models can produce anomalous results, such as negative flows.

[10] Daily streamflow generation models originally employed the AR model as well, typically with a lag-1 or lag-2 process [*Beard*, 1967; *Quimpo*, 1968; *Quimpo and Yevjevich*, 1967; *Payne et al*., 1969]. However, the characteristic hydrograph shape, with its intermittent, highly skewed storm pulses and gradual recession, is difficult to reproduce using autoregressive models without significant modifications [*Sharma et al*., 1997]. Several methods have since been proposed which maintain historical distributions while better approximating natural hydrograph shapes, including disaggregation schemes and shot noise (SN)/Markov Chain models.

[11] Disaggregation schemes begin with monthly or annual models, such as ARMA, and then apportion flows to create daily or weekly series. Original parametric disaggregation models used statistical parameters from historic time series to temporally disaggregate annual flows [*Valencia and Schakke*, 1973; *Stedinger and Vogel*, 1984; *Maheepala and Perera*, 1996]. In large systems, this type of model can quickly become over-parameterized [*Grygier and Stedinger*, 1988]. More recent approaches to disaggregation operate on the principle of resampling. The method of fragments, originally proposed by *Harms and Campbell* [1967], resamples short duration fragments of the historical record [*Srikanthan and McMahon*, 1982] or synthetically generated hydrographs [*Porter and Pink*, 1991] and scales them to match monthly or annual sums. Nonparametric techniques such as moving block bootstrapping [*Vogel and Shallcross*, 1996] or K-Nearest Neighbor models [*Lall and Sharma*, 1996; *Prairie et al*., 2006; *Buishand and Brandsma*, 2001] have been applied more recently to identify appropriate fragments.

[12] SN models were introduced to produce a more realistic daily hydrograph by modeling the in-stream response produced by a pulse, corresponding to a storm event. In the original SN streamflow models, *Weiss* [1977] modeled rainfall occurrences as a Poisson process, with intensities following an exponential distribution. Watershed response is also modeled exponentially, with separate transfer functions for base flow and direct runoff. *Treiber and Plate* [1975] extended this model using transition (Markov) probabilities to control pulse and recession days and a transfer function which convolved pulses to generate runoff. *Sargent* [1979] condensed this method, focusing on a more conceptual model of runoff generation, using a modified exponential distribution for pulse heights and an exponential decay for recession curves.

[13] The SN-Markov chain model is more physically consistent with hydrologic processes, is capable of maintaining flow characteristics at the monthly and annual aggregated scale, and performs favorably when compared to other models [*Chapman*, 1997]. This general model formulation has since been used to generate synthetic daily streamflows in a wide range of hydrologic scenarios

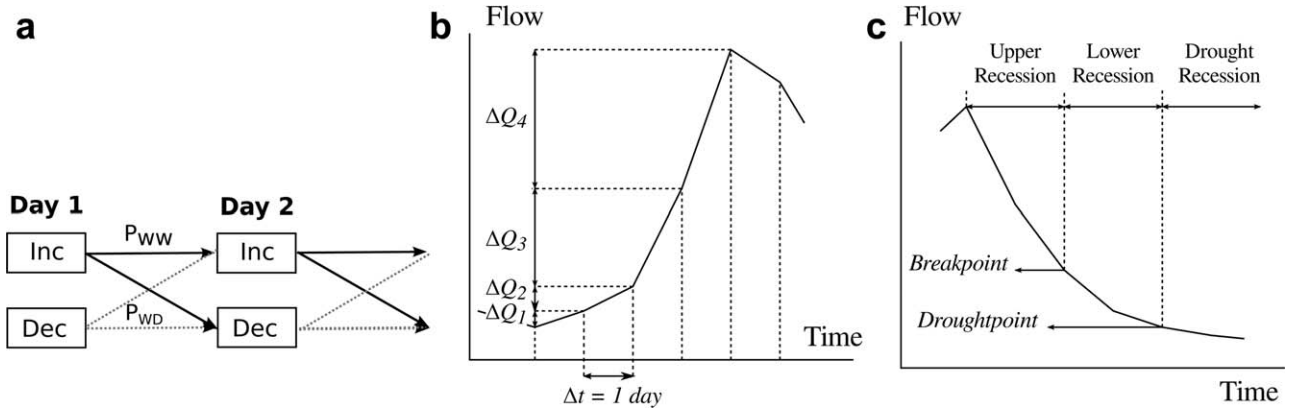

Figure 1. (a) Daily Markov state transition, (b) increasing limb, and (c) decreasing limb.

[*Kottegoda*, 1980] including intermittent streams [*Aksoy and Bayazit*, 2000; *Aksoy*, 2003] and multiple sites [*Szilagyi et al*., 2006].

2.2. Climate Change and Streamflows in the Mid-Atlantic

[14] Climate research suggests that the Earth's climate is changing due to human activities, which alter the composition of the global atmosphere, increasing levels of carbon dioxide and other greenhouse gases [*Meehl et al*., 2007b]. All scenarios assessed by the Intergovernmental Panel on Climate Change (IPCC) project increases in global mean surface air temperature, with scenarios beginning to diverge by the end of the next century (2090–2100) [*Meehl et al*., 2007b].

[15] Climate projections in the Mid-Atlantic region predict moderate increases in mean annual temperature, precipitation, and streamflow over the next century [*Najjar et al*., 2009; *Pyke et al*., 2008; *Hayhoe et al*., 2008; *Meehl et al*., 2007b]. An evaluation of the four best performing GCMs in the Chesapeake Bay watershed suggests an increase in mean annual temperature of 3.9 ± 1.1°C and an increase in precipitation of 9 ± 12% by the end of the century under the most severe A2 scenario [*Najjar et al*., 2009]. This continues the historical trend of precipitation increases throughout the northeast United States during the 20th century [*Groisman et al*., 2001, 2004]. *Milly et al*. [2005] predict a 3.6% increase in mean annual streamflow (SRES A1B) for the 2041–2060 period in the Mid-Atlantic, with 55–70% of GCM models showing an increase in flow by this time period. Variability in these results follows the pattern outlined in *Matalas* [1997], with the greatest confidence in temperature models, followed by precipitation and ultimately streamflow, which shows the highest uncertainty.

[16] Despite projected increases in mean annual precipitation and flow for the Mid-Atlantic, variation in the distribution and seasonality of precipitation and runoff is potentially more important for water resources management. Storm events in the region are projected to become both more severe and intermittent, with precipitation intensity expected to increase by one standard deviation along the east coast of the United States by the end of the 21st century, concurrent with a decrease in the total number of storm events [*Meehl et al*., 2007b]. The annual number of dry days in the region is projected to increase by 0.25–0.5 standard deviations by 2100 [*Tebaldi et al*., 2006]. This increase in dry days, combined with an increase in heat waves, defined as consecutive days with temperatures at least 5°C higher than daily norms, will likely produce longer and more pronounced droughts for the region [*Meehl et al*., 2007b].

[17] These projections suggest a moderate increase in mean flows, with greater likelihood of both flooding, due to storm intensity, and drought, due to prolonged dry periods. Seasonality is also expected to shift, with the greatest increase in precipitation occurring during the winter and spring [*Najjar et al*., 2009]. Similar seasonal trends were noted in *Mccabe and Ayers* [1989], *Moore et al*. [1997], and *Hayhoe et al*. [2008].

3. Model Definition

3.1. Model Overview

[18] The proposed model is designed to simulate daily streamflows under both current and potential future climate conditions. It is a combination of a monthly climate model, which generates climate based on the likelihood of discrete climate-streamflow states, and a daily streamflow model, which generates hydrographs based on parameters tied to the climate-streamflow state.

3.2. Daily Streamflow Model

[19] The daily streamflow generation model consists of two parts: (i) determination of the river's state, i.e., increasing or decreasing streamflow and (ii) calculation of the ascension or recession curve based on this state. A two-state Markov chain is employed to determine whether flow is increasing (wet) or decreasing (dry) on a given day. The Markov chain is assumed to be first order, depending only on whether the previous day was "wet" or "dry," and can be represented by the transition probability matrix:

$$P = \begin{bmatrix} P_{dd} & P_{dw} \\ P_{wd} & P_{ww} \end{bmatrix}$$

[20] where P_{dd} is the probability of a dry day provided that the previous day was dry, P_{dw} is the probability of a wet day given the previous day was dry, P_{wd} is the probability of a wet day following a dry day, and P_{ww} is the probability of a wet day following a dry day (Figure 1a).

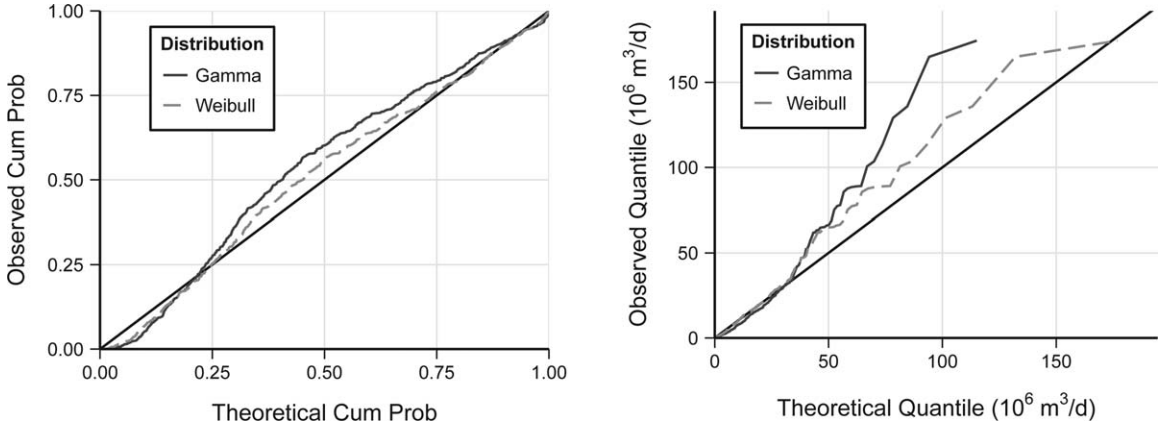

Figure 2. Example P-P (left) and Q-Q (right) plots for the increasing limb in the Potomac River during May. The two-parameter gamma distribution is shown as a solid line, while the Weibull distribution is shown as a dashed line.

[21] The ascension limb of the daily hydrograph, occurring on wet days, is simulated by randomly generating daily flow increases, ΔQ, from a Weibull distribution (Figure 1b). The Weibull distribution was found to provide the best fit to flow increments in the Potomac data set (Figure 2), mirroring results in *Szilagyi et al*. [2006]. Goodness of fit was determined based on log likelihood and the Bayesian information criterion. The two-parameter gamma distribution used in *Aksoy* [2003] was also tested but was found to provide a poor fit to the data (Figure 2). Selection of the Weibull distribution is reasonable, given its success in similar studies [*Szilagyi et al*., 2006] and its use in many other hydrologic applications as an extreme value distribution with a relatively flexible shape parameter. Randomly generated increment values are then ranked in increasing order from smallest to largest increment, which occurs at the hydrograph peak. This preserves the correlation structure of the ascension curve and the characteristic shape of daily hydrographs [*Aksoy*, 2003].

[22] The recession curve, occurring on dry days, is modeled as exponential decay, which is a simple, yet generally accepted form for baseflow recession [*Tallaksen*, 1995] (Figure 1c):

$$Q = Q_o e^{-bt} \tag{1}$$

[23] Previous studies have separated streamflow recession into two portions (upper and lower) with unique recession coefficients [*Sargent*, 1979; *Aksoy*, 2003; *Szilagyi et al*., 2006]. These recession equations take the form,

$$Q = Q_o e^{-b_{\text{upper}}\, t} \tag{2}$$

$$Q = Q^* e^{-b_{\text{lower}}\,(t-t^*)} \tag{3}$$

where b_{upper} is the upper recession coefficient, b_{lower} is the lower recession coefficient, Q_o is the preceding peak flow, Q^* is the initial flow in the lower recession, t is the number of days after the peak, and t^* is the time from the start of the lower recession. Conceptually, the upper coefficient describes recession following a large storm event, which is primarily influenced by channel storage, while the lower coefficient models baseflow recession, which is influenced by groundwater storage. Rather than employing an arbitrary splitting criterion, like the monthly mean flow [*Aksoy*, 2003] or the 90% ratio [*Sargent*, 1979], breakpoints were selected iteratively to minimize the sum of squared error for the upper and lower recession curves.

[24] Because the purpose of this model is to generate daily streamflow scenarios for use in water resources planning and drought management, greater attention was paid to low flow modeling. With this in mind, a third recession coefficient was added to model extreme low flow recession:

$$Q = Q_{\text{drought}}\, e^{-b_{\text{drought}}\left(t - t_{\text{drought}}\right)} \tag{4}$$

where b_{drought} is the drought recession coefficient, Q_{drought} is the initial flow during drought recession, and t_{drought} represents time from the start of the drought recession. This addition considerably improved low flow accuracy, preventing flows from approaching zero during extreme low flow events. Inclusion of an additional term is reasonable in the Potomac River application given that previous uses of the model focused on intermittent streams, where zero flow is expected [*Aksoy*, 2003]. The extreme low flow criteria point was set at the 5% low flow exceedance level by maximizing goodness of fit and confirmed visually using flow-duration curves. The drought recession coefficient is assumed to be equal for all climate states, as it depends only on baseflow and river stage. The low flow drought condition is experienced very rarely, with only 56% of years in the historical record (1931–2007) falling below this level at any point, typically only for 1–5 days.

3.3. Monthly Climate Model

[25] Simulation of the monthly climate-streamflow states is governed by a first-order Markov chain, with transition probabilities derived from the historical record. Monthly climate-streamflow states may be tied to temperature, geopotential heights, precipitation, humidity, or any number of climate indices. Classifying monthly climate into discrete states is common in synoptic atmospheric research and has been used to correlate global climate indicators with local weather cycles [*Kalkstein et al*., 1987; *Yarnal and Draves*, 1993;

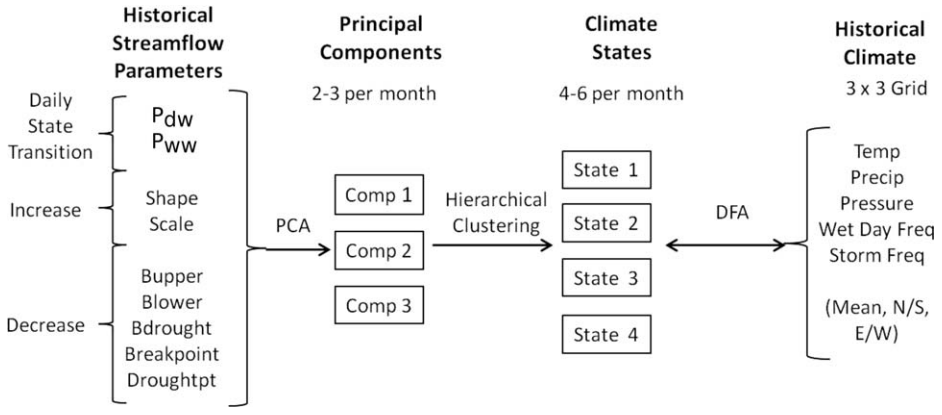

Figure 3. Streamflow analysis and model-fitting procedure.

Michelangeli et al., 1995; *Huth*, 1999]. Several climate generation models use Markov chains to describe climatic patterns, either explicitly through circulation typing or implicitly using hidden Markov models [*Hughes and Guttorp*, 1994; *Bellone et al*., 2000; *Thyer and Kuczera*, 2003; *Sansom and Thomson*, 2007]. In this manner, the proposed method is similar to statistical downscaling and uses common statistical techniques to link GCM-scale climate to finer resolution phenomena. While the mathematical principles are similar, there are important differences in their purposes. Statistical downscaling relates a particular GCM simulation to climate at a finer resolution and/or corrects for model bias. The proposed method instead uses GCM output to classify months into discrete states and then calculates the transition probability between these states. The effects of climate change are then simulated by adjusting the Markov transition probabilities based on future GCM scenarios, mirroring shifts in monthly climate patterns. In this way, the original GCM simulation time series is not used directly to generate streamflow.

[26] During the analysis process (Figure 3), principal component analysis (PCA) [*Hotelling*, 1933] is used (i) to investigate patterns in variation within the daily streamflow model parameters and (ii) to condense these parameters into a smaller set of components that are mutually orthogonal. PCA is commonly used in climatology in this manner to condense and normalize multivariate climate data prior to clustering [*Corte-Real et al*., 1999]. It is particularly useful when variables are highly correlated, as is the case with streamflow parameters P_{dw}, P_{ww}, shape, scale, b_{lower}, b_{upper}, and the recession breakpoint.

[27] The resulting normalized and orthogonal components are grouped using a hierarchical [*Ward*, 1963] clustering algorithm in JMP statistical software (JMP, version 7, SAS Institute Inc., Cary, NC, 1989–2007). Ward's method minimizes the within-cluster sum of squares at each cluster step, while merging clusters based on the squared distance between the new centroid and the two original centroids, weighted by the number of observations [*Ward*, 1963]. Ward's clustering was selected after initial comparisons with K-means clustering showed that Ward's clustering was more capable of handling outliers and allowed for better interpretation and selection of optimal clusters through the dendrogram.

[28] Clustered streamflow parameters are then related to large-scale climate indices using historical GCM data. This analysis is performed using discriminant function analysis (DFA), a statistical method used to determine the set of continuous variables that best assigns observations to predetermined groups. In this instance, DFA is used to identify the combination of 15 potential climate measures that best classifies membership to the monthly climate states determined through clustering. Variables are tested for inclusion in a stepwise manner based on Wilk's lambda, a measure of separation between the centroids. The resulting predictive equation uses the Mahalanobis distance of each observation to the cluster centroid. This distance is of the form:

$$D^2 = (x - \bar{x}_j)' \hat{V}_j^{-1} (x - \bar{x}_j) \tag{5}$$

where D^2 represents the Mahalanobis distance, x represents the point in question, $\bar{x}_j$ is the jth centroid, and $\hat{V}_j$ is the covariance matrix. The resulting discriminant equation uses the Mahalanobis distances to calculate the probability of membership to a particular class based on the sum of the negative exponentials of the distances. For instance, the discriminant function for membership to class 1 is as follows:

$$P(1/x) = \frac{1}{1 + e^{-\frac{1}{2}\left(D_2^2 - D_1^2\right)} + e^{-\frac{1}{2}\left(D_3^2 - D_1^2\right)} + \cdots} \tag{6}$$

3.4. Generating Historical and Climate-Adjusted Streamflows

[29] To generate historical or climate-adjusted daily streamflows based on GCM simulations, the analysis process is reversed: (i) discriminant functions obtained through historical analysis are used to classify future GCM realizations into monthly climate-streamflow states, (ii) new climate state transition probabilities are calculated, and (iii) the daily flow model is executed using the newly adjusted climate-streamflow state transition probabilities and historical flow parameters associated with each state.

[30] Accuracy of this process may be validated by analyzing and simulating flows based on the historical record. In this case, the discriminant functions are used to reclassify historical months into climate states, allowing for misclassification due to errors in the discriminant functions. Transition probabilities are then obtained, daily streamflows generated, and results compared with the true

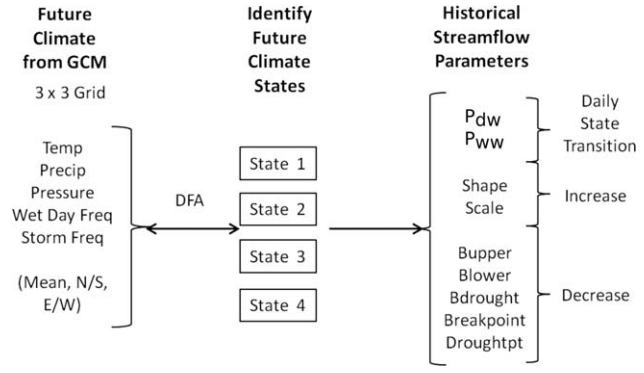

Figure 4. Streamflow generation procedure. Mean refers to the area-weighted mean, N/S refers to the North/South trend, and E/W refers to the East/West trend.

historical time series at daily, monthly, and annual scales. This step provides both validation of the model and generates a baseline model, against which the climate-adjusted results can be compared (Figure 4).

4. Results

4.1. Data Preparation

[31] The Potomac River was used as a case study to demonstrate the capabilities of the proposed stochastic streamflow generation method. Flows were analyzed and simulated for USGS stream gauge 01646500, located on the Potomac River near the Little Falls pumping station in Washington, D. C. A daily record of streamflows between 1 October 1929 and 30 November 2007 was obtained from the Interstate Commission on the Potomac River Basin (ICPRB). This dataset was adjusted by the ICPRB to reflect historic flows in the Potomac River without the effects of human interaction, calculated by adding daily river withdrawals and mathematically removing reservoir releases from the historical record [*Ahmed et al*., 2010]. This adjustment compensates for the effects of increasing population and development, allowing for more accurate comparisons across a long time series. The effects of land-use change on streamflow were initially considered; however, this impact was found to be minor [*Stagge and Moglen*, 2011] in relation to uncertainty in streamflow simulation and was therefore not included in this study. The small effect of land-use change on Potomac flows is attributed to the watershed's large size and the offsetting trends of urban and suburban development and agriculture to forest conversion [*Stagge and Moglen*, 2011]. The effect of land-use change could be more significant for smaller, more flashy watersheds.

[32] Both monthly and daily historical climate data were obtained from the NOAA-CIRES 20th Century Reanalysis (V2) data set, made available by NOAA and the U.S. Department of Energy [*Compo et al*., 2011]. Grid dimensions (2.0° latitude × 2.0° longitude) are comparable to available climate-adjusted GCM datasets, which reduces the likelihood of scaling effects.

[33] Five GCMs (Table 1) were used to simulate climate-adjusted streamflows. Each GCM is based on the IPCC's AR 4 round of climate models and was accessed via the WCRP CMIP3 Multi-Model data portal [*Meehl et al*., 2007a]. For all GCMs, climate variables identical to the historical climate data set were used, with historical climate represented by the Climate of the 20th century (20C3M) scenario, and potential future climate simulated by the SRES A1b, A2, and B1 emission scenarios. Current conditions were simulated based on the 1961–2000 time period, while future climate scenarios were separated into three segments of equal duration: 2010–2039, 2040–2069, and 2070–2099.

4.2. Fitting the Daily Streamflow Model

[34] Parameters of the daily streamflow model were fit to each month in the historical record individually, with each day classified as either increasing, "wet state" or decreasing, "dry state." State transition probabilities were calculated as:

$$P_{ij} = \frac{n_{ij}}{\sum_j n_{ij}}, \qquad i,j = w,d \tag{7}$$

where n_{ij} represents the number of observed transitions from state i to j. Wet day increments for each month were fit using the Weibull distribution based on maximum likelihood estimation by the "fitdistrplus" package in R (version 2.12.0) [*Delignette-Muller et al*., 2010]. Goodness of fit was summarized using the Bayesian information criterion. Dry day recession coefficients were calculated using nonlinear least-squares estimation (R-"nls" package). Flows were then ranked and all potential breakpoints tested iteratively to determine the optimal splitting criterion between the upper and lower recession curves.

[35] The two transition probabilities of the daily flow model operate in tandem to describe the frequency and duration of the increasing limb, with P_{dw} analogous to storm frequency and P_{ww} analogous to storm duration. As would be expected for the region, the winter and early spring is characterized by low frequency, long duration events (low $P_{dw,}$ high P_{ww}), while the summer and early fall months are characterized by high frequency and short duration events (high $P_{dw,}$ low P_{ww}) (Figure 5a).

[36] Recession coefficients control the streamflow recession rate for three distinct flow zones, with b_{upper} related to recession following large storm events, b_{lower} baseflow

Table 1. Evaluated Global Climate Models (IPCC-AR4)

Model	Institution	Location	Reference
CCSM3	National Center for Atmospheric Research (NCAR)	USA	*Collins et al*. [2006]
CGM_3.1	Canadian Centre for Climate Modeling and Analysis	Canada	*Flato* [2005]
CSIRO_MK3	CSIRO Atmospheric Research	Australia	*Gordon et al*. [2002]
MIROC_3.2	Center for Climate System Research	Japan	*Watanabe et al*. [2011]
PCM1	National Center for Atmospheric Research (NCAR)	USA	*Washington et al*. [2000]

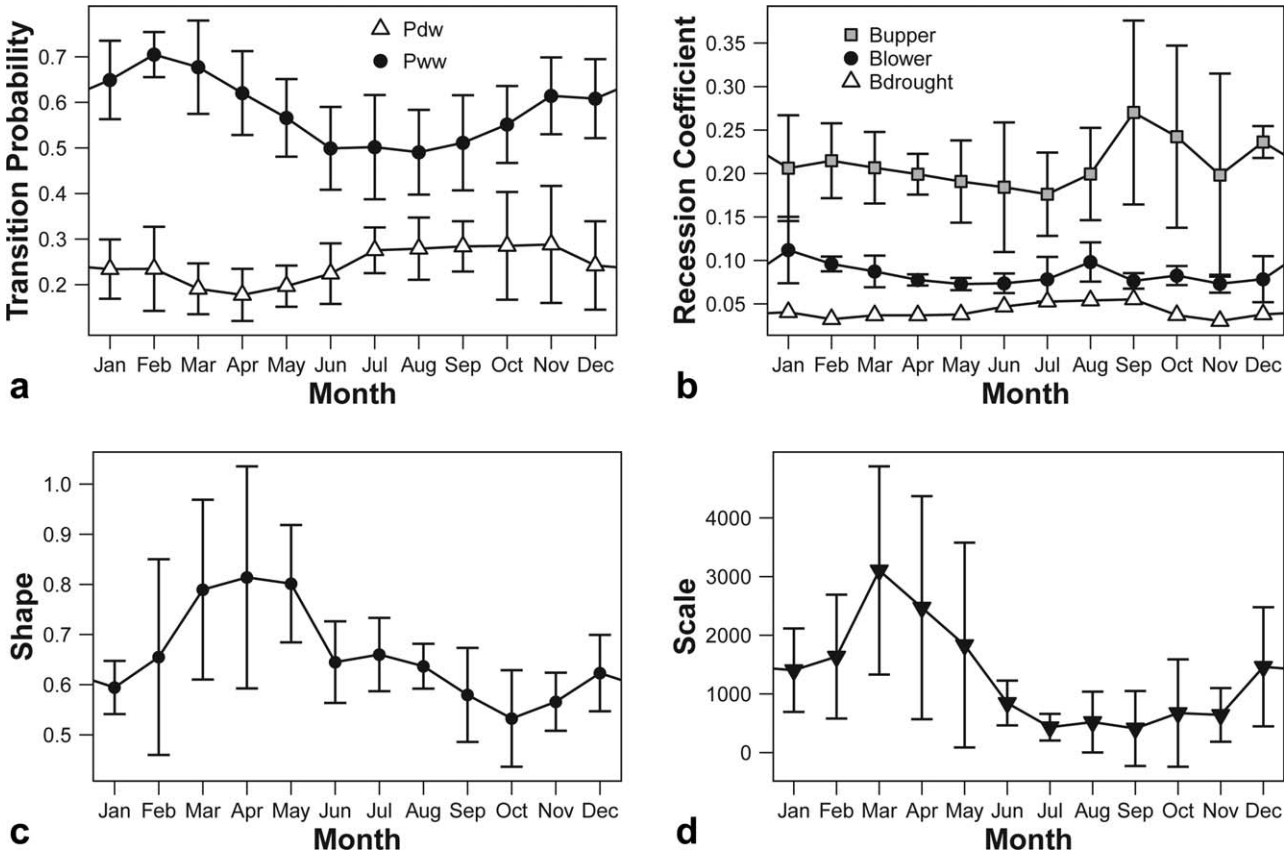

Figure 5. Daily streamflow model parameters. Line represents mean parameter, while errors bars signify standard deviation. (a) Transition probability, (b) recession coefficient, (c) increasing limb shape, and (d) increasing limb scale.

recession, and b_{drought} related to recession during extreme low flows. As expected, the recession coefficients affiliated with groundwater storage show considerably less variability than b_{upper} (Figure 5b). Recession coefficients decrease during the spring recharge period as more groundwater is available for baseflow, slowing recession rates. Alternatively, the large peak in b_{upper} during the fall coincides with the lowest annual groundwater levels.

[37] The scale and shape parameters of the Weibull distribution control the magnitude and flashiness of the increasing limb, respectively. Low shape parameter values correspond to a more flashy flow distribution, with more extreme high flow increments and also more increments near zero. These low shape values occur during the summer and early fall, when rain events tend to be convective, short, and severe (Figure 5c). In contrast, the late winter and spring are characterized by high shape parameters, corresponding to more frontal storm events. The scale parameter is related to the magnitude of storm events and, as such, mirrors the general shape of monthly flows in the Potomac River, with peaks in March and April and lowest values in September and October (Figure 5d).

4.3. Extracting Principal Components from Model Parameters

[38] Because of scaling issues and the potential for correlation among the streamflow parameters (P_{dw}, P_{ww}, shape, scale, b_{lower}, b_{upper}, and recession breakpoint), PCA was used to calculate a smaller set of normalized, orthogonal summary statistics. The scale parameter and the breakpoint between upper and lower recession curves were adjusted using a logarithmic transform prior to being normalized because of their highly skewed nature.

[39] Three stopping criteria were used for PCA: the Kaiser-Guttman criteria (eigenvalues $\lambda > 1$) [*Guttman*, 1954; *Kaiser*, 1960], the Scree plot [*Cattell*, 1966], and Parallel Analysis [*Horn*, 1965]. Agreement among these tests was typical and resulted in 2–3 components being retained for each month. Approximately 60–81% of the standardized variance was explained by these components. Across most months, the first eigenvector explained 38–50% of the variance, with predominant loadings from the recession coefficients, breakpoint, and scale parameters, each in the same direction. The second component generally explained 17–31% of the variance and typically took loadings from the state transition probabilities, P_{dw} and P_{ww}, in opposing directions. Where present, the third component explained 15–17% of the overall variance, with loading solely from either P_{ww} or the shape factor. There was no discernible temporal pattern in loading or in variance explained.

4.4. Clustering Monthly Climate-Streamflow States

[40] Following PCA, the resulting normalized, orthogonal components were grouped using a hierarchical [*Ward*, 1963] clustering algorithm in JMP statistical software

Table 2. Climate Variable Discriminating Power[a]

		Jan	Feb	Mar	Apr	May	Jun	Jul	Aug	Sep	Oct	Nov	Dec
Misclassified (%)		33.8	31.0	32.4	39.4	42.3	33.8	14.1	26.8	19.7	19.4	22.2	31.9
Cross-Val (%)		42.0	42.6	41.3	31.0	42.0	41.2	37.1	29.3	22.3	41.7	29.5	27.4
Number of Variables		5	5	5	5	5	5	5	6	7	7	6	5
STemp	Mean							3			4	2	
	N-S								3		7		
	E-W					5	5				6		
SPress	Mean			2	5				5				
	N-S		4	4				2		4	3		4
	E-W	1	2			4	1						
Precip	Mean	2	1	1	1	1		1	1	1	1	1	1
	N-S							5		5			3
	E-W	4			3				6	6	2	3	5
WetDay	Mean	3	3	3		3	3			2			
	N-S				2		2	4	4	3		6	2
	E-W		5	5								4	
StormFrq	Mean	5			4	2	4						
	N-S									7	5		
	E-W								2			5	

[a]Numbers refer to the rank order in which the variables enter the discriminating equation. Underlined values represent a climate predictor variable that has statistically significant discriminating power ($p < 0.05$) in the final discriminant functions. Percent misclassified is shown as a percent for the entire model and the 10% holdout cross-validation set with 500 iterations.

(JMP, version 7). Clustering showed a slight temporal trend, with the winter and spring months tending toward more (5–6) distinct clusters and the summer tending towards fewer (4) clusters. Greater variability in flow regimes during the winter and spring months may be caused by a wider variety of complicating climate factors, including snowmelt and long-term groundwater storage.

4.5. Creating Predictors of Climate-Streamflow States

[41] Clusters of historical streamflow regimes were then related to historical climate using DFA. Potential climate variables considered in this study include mean monthly surface temperature (K), mean monthly surface pressure (Pa), mean monthly precipitation rate (kg m^{-2} s^{-1}), monthly wet day frequency (%), and individual storm frequency (%). Wet day frequency is the ratio of days with measurable (>0.25 cm) rainfall to total days in a month, while individual storm frequency is the ratio of unique rainfall events to total days in a month. These two measures describe the frequency and duration of rainfall events in a given month. To avoid issues at monthly boundaries, ongoing storm events that began prior to the first day of a month are considered a unique storm event.

[42] Variables involving precipitation were chosen based on their direct relevance to surface hydrology. This is in contrast to statistical downscaling techniques, which similarly relate coarse GCM output to finer resolution climate and most often rely on circulation-based predictors, such as geopotential height [*Bardossy and Plate*, 1992; *Wilby and Wigley*, 2000]. Use of GCM precipitation has been avoided as a downscaling predictor because it is derived based on parameterizations of other GCM simulated variables [*Dai*, 2006] and because validation studies have shown only moderate predictive skill when compared with other modeled GCM variables [*Lau et al*., 1996; *Mearns et al*., 1995]. However, recent research has proposed that while precipitation may be modeled less accurately, the use of GCM precipitation has the advantage of integrating the complex physical precipitation processes that use of circulation indices alone may not [*Maurer and Hidalgo*, 2008; *Widmann et al*., 2003]. Parameterization of GCM precipitation is most reliable when considered at the monthly scale, coarse spatial resolution (≈500 km), and normalized [*Eden et al*., 2012; *Widmann and Bretherton*, 2000] as in this study, further supporting the use of normalized monthly precipitation as a potential discriminating variable. Future research may explore the value of also including tropospheric circulation variables as discriminating variables.

[43] For each of these five climate variables, three measures were used to summarize climate across the 3 × 3 spatial grid: watershed area-weighted mean, north to south (N-S) gradient, and east to west (E-W) gradient. This simplification resulted in 15 potential discriminating variables.

[44] All climate predictor variables were based on normalized anomalies relative to each GCM's historical reanalysis (20C3M), accounting for consistent model bias. While variables such as monthly wet day frequency or storm event frequency tend to have more uncertainty in GCM simulations than atmospheric circulation, their use as predictor variables in this model is related to their direct impact on streamflow regime. These predictor variables satisfy the assumption of normality in DFA, although violations of this assumption do not tend to affect results significantly [*Tabachnick and Fidell*, 2007]. This was confirmed using the Shapiro-Wilk test for normality, which produced p values ranging from 0.17 to 0.78. The largest deviations from normality occurred for the directional variables (N/S, E/W) at seasonal transitions. Climate predictor variables were selected in a stepwise fashion, evaluating the entire model at each step against Wilks' lambda (Λ) (F test) and the relative percent misclassified. Percent misclassified data were used to confirm the discriminating power of the climate variables and ranged from 14% to 42% (Table 2). To check against overfitting, cross validation was run via repeated random subsampling, using a 10% holdout validation set randomly selected across 500 iterations. Results of

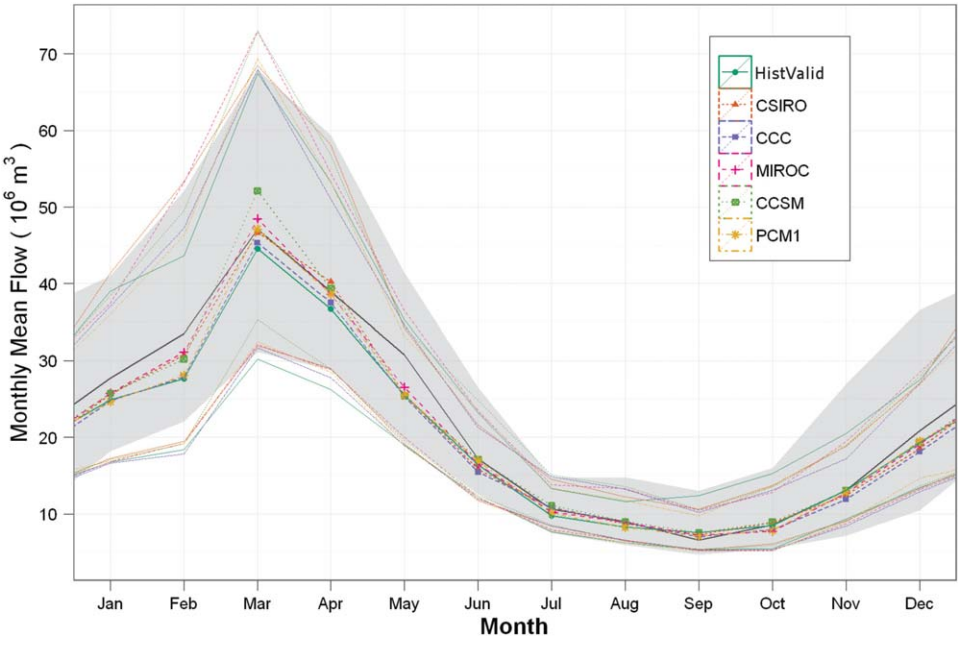

Figure 6. Monthly mean flows for the historical scenario (1961–2000). Median values are displayed as central lines, with black representing the historical record and colored lines representing the various models. The 25th and 75th percentiles are represented by the shaded area for the historical record and thin lines for model simulations.

this cross validation are also presented in Table 2 and do not differ significantly from the fit miscalculation rate, implying a robust discriminant model. Press's Q goodness of fit is statistically significant ($p < 0.05$) for all discriminant functions, suggesting that they are capable of classifying months based on the given climate predictors. The most accurate discriminant functions occur during the summer months, while the worst fit occurred in the winter and spring. This trend suggests that streamflow during the winter and spring is partially related to variables other than the immediate climate, such as snowmelt or groundwater recharge. Flow regime during the summer is less dependent on these extraneous variables and is more readily explained by more recent climate.

[45] Other trends are apparent among the discriminating power of the climate variables (Table 2). Mean monthly precipitation rate is significant for nearly all months and typically explains the most variability for each month. Area-weighted mean monthly precipitation is important during winter and spring, when most precipitation occurs as large, frontal events; however, the directional components (N-S, E-W) become significant in late summer and early fall as storm events become more spatially fragmented. Number of days with measurable rainfall (WetDay) is the second most consistent climate indicator, present in the majority of discriminant functions and following a similar pattern as total precipitation, with the area-weighted mean dominating winter and spring and directional components dominating during summer. Atmospheric pressure is a significant climate indicator both during the mid-winter and summer. Atmospheric pressure during the summer likely functions as an indicator of convective storm events. Temperature and unique storm events (StormFrq) tend to have the least discriminating power; however, mean monthly temperature becomes significant during the summer months.

4.6. Simulation of Historical Streamflow

[46] Historical flow sequences were generated using the Climate of the 20th Century (20C3m) scenarios for each GCM and compared against the observed historical record in order to validate the streamflow generation method and to identify any bias introduced by the climate models. Streamflow simulated using this method successfully reproduced the observed historical record closely at the daily, monthly, and annual time steps. Simulation using the MIROC, CSIRO, and NCAR CCSM models was consistently the best across all metrics, while the NCAR PCM1 and CCC models generally produced poorer statistical agreement. As a general rule, agreement was best during months with consistent climate, whereas months at the seasonal transitions produced greater errors.

4.6.1. Seasonal Trends

[47] The model successfully reproduces the monthly seasonal pattern of the Potomac River when run using transitional probabilities calculated directly from the true historical record, the HistValid set (Figure 6). This model validation set suggests that the model itself does not have any systematic seasonal biases. When flows are instead simulated using transition probabilities calculated from 20th century GCM realizations, each GCM also adequately reproduces historical seasonality among monthly aggregated flows on the Potomac River (Figure 6). Across all months, the GCM with the most consistent agreement is the MIROC model. The CSIRO and NCAR CCSM models were also capable of reproducing the central tendency and distribution of monthly means (Table 3). The PCM1 and CCC models perform adequately for the majority of

Table 3. Mann-Whitney Test for Historical Validation of GCM Means[a]

	Annual		Monthly											
	Mean	CV	Jan	Feb	Mar	Apr	May	Jun	Jul	Aug	Sep	Oct	Nov	Dec
HistValid	0.10	0.078	0.37	0.04	0.09	0.20	0.11	0.40	0.46	0.72	0.25	0.92	0.72	0.11
CCC	0.02	0.02	0.23	0.07	0.15	0.27	0.10	0.17	0.57	0.25	0.96	0.54	0.20	0.05
CSIRO	0.15	0.05	0.52	0.31	0.19	0.94	0.07	0.17	0.67	0.43	0.63	0.70	0.43	0.06
MIROC	0.20	0.12	0.35	0.38	0.43	0.50	0.25	0.41	0.87	0.29	0.65	0.54	0.50	0.08
CCSM	0.30	0.05	0.38	0.26	0.80	0.67	0.09	0.76	0.47	0.20	0.59	0.72	0.52	0.10
PCM1	0.04	0.06	0.19	0.09	0.27	0.42	0.06	0.52	0.60	0.70	0.99	0.57	0.45	0.09

[a]Test statistic is the Mann-Whitney p value. Underlined values indicate a statistically significant difference from the historical.

months, with some deviation occurring due to an underestimate of median and high flows. Variance among months with low flows was the most successfully modeled monthly parameter, likely due to the emphasis on drought modeling in the model's development.

[48] Monthly agreement is best for mid-seasonal months across all GCM models, with greater error at seasonal transitions. Agreement during summer and early fall (June to October) is best, with Mann-Whitney p values between 0.168 and 0.990, suggesting no statistical difference in mean monthly flows (Table 3). All GCMs underestimate the median for February ($p = 0.039$–0.384) but match the distribution well (Kolmogorov-Smirnov $p = 0.042$–0.343) (Figure 6). Likewise, the distribution of monthly flows in May agree well with the historical record but tend to underestimate the median. November and December have good agreement with regards to the median and low flows, with some underestimates of the upper limb of the distribution (Figure 6).

4.6.2. Annual Statistics

[49] At the annual time step, several statistics are reproduced successfully, including the annual mean, coefficient of variation (CV), date of minimum flow, and date of maximum flow. The validation set, HistValid, using the true historical transition probabilities, showed no statistical difference between the distribution of annual mean flows and the historical ($p = 0.103$). Additionally, no statistical difference exists for the MIROC, CSIRO, and CCSM models ($p = 0.151$–0.301) between the GCM-generated distribution of annual mean flows and the observed historical, while the CCC and PCM1 models exhibit a slight statistical difference ($p = 0.023$–0.039), attributed to underprediction (Table 3). The distribution of annual CV is also reproduced well for all GCMs ($p > 0.05$), except for the CCC model ($p = 0.024$) (Table 3).

[50] The date of the annual minimum and maximum, with medians of 28 September and 7 March, respectively, is well simulated by all GCMs and the validation set. Dates were adjusted based on water year (1 October to 30 September) for maximum flow and low flow year (1 April to 31 March) to prevent discontinuities. In the historical record and simulations, the date of the minimum flow has significantly less variation than the date of the maximum flow.

[51] While the various GCM-based models produce a slight bias in the distribution of annual minimum flow for the wettest years, all models reproduce extreme low flows (recurrence interval <3 years) very well. While this limitation should be considered when using the model, it is important to note that years with greater than average low flows are of less consequence for low flow modeling, and the $7Q_{10}$ is a much more useful measure for simulating drought operations. All GCMs have similar performance with respect to extreme low flows, except for the PCM1 model, which tends to predict more severe low flows than the true historical record.

4.6.3. Daily Flow Distribution

[52] Daily streamflow distributions and dynamics, typically the most difficult to replicate in streamflow generation models, are reproduced well by the proposed stochastic model. The model captures much of the daily variability, successfully simulates the distribution of daily flows, and replicates the daily streamflow autocorrelation structure. As with monthly aggregated flows, the best agreement occurs during months with relatively stable climate, rather than during transitional seasons, hence the distribution of daily flows is most consistent for January and the summer months (June, July, and August).

[53] The MIROC and CSIRO GCMs produce the most consistent agreement for the daily flow distribution (Table 4). The remaining models perform well for most months, while some isolated months exhibit a slight bias across the flow duration curve. The CCSM model agreement is good in all aspects, except for predicting high flow events occurring in September and October (hydraulic alteration $> 10\%$). The PCM1 and CCC GCMs both

Table 4. Percent Hydrologic Alteration of 20th Century GCM Flow Distributions Using 5 Percentile Flow Bins

Model	Annual	Jan	Feb	Mar	Apr	May	Jun	Jul	Aug	Sep	Oct	Nov	Dec	Mean
HistValid	1.0	2.6	7.3	10.4	9.9	6.6	3.4	3.5	4.7	3.5	7.4	10.7	9.8	6.6
CCC	1.7	3.9	6.5	8.4	8.9	8.3	2.9	3.9	5.0	10.8	8.3	12.9	10.3	7.5
CSIRO	1.5	3.6	5.4	8.8	9.7	7.7	4.6	4.4	5.4	5.4	9.3	12.2	9.9	7.2
MIROC	0.8	4.1	7.6	8.1	8.4	6.5	4.8	2.7	3.6	6.4	7.2	9.5	7.3	6.3
CCSM	1.1	4.8	6.5	6.7	8.3	6.6	5.4	2.4	4.9	10.6	10.0	9.8	6.4	6.9
PCM1	1.1	4.1	7.4	9.2	9.6	7.9	3.1	2.1	4.3	9.2	7.7	12.3	10.7	7.3
Mean	1.2	3.9	6.8	8.6	9.1	7.3	4.0	3.2	4.7	7.7	8.3	11.2	9.1	

Table 5. Percent Change in Mean Annual Flow for Climate Change Realizations

Model	2010–2039	2040–2069	2070–2099
CCC	3.73 (2.62–4.37)	3.34 (−0.11 to 5.98)	5.04 (3.20–7.47)
CCSM	0.50 (−2.29 to 2.50)	3.54 (1.86–5.08)	3.89 (0.70–6.49)
CSIRO	0.19 (−3.09 to 6.47)	2.35 (1.15–4.03)	0.68 (−4.88 to 9.64)
MIROC		2.23 (1.37–3.25)	3.10 (−1.13 to 6.88)
PCM1	6.23 (5.66–6.79)	8.58 (7.42–9.59)	8.60 (7.78–9.27)

successfully reproduce the daily flow distribution for all months, except for winter, where they underpredict the middle of the flow duration curve (50–75% exceedance probability). Across all months, the CCSM model tends to be the "wettest" model, producing consistently higher flow

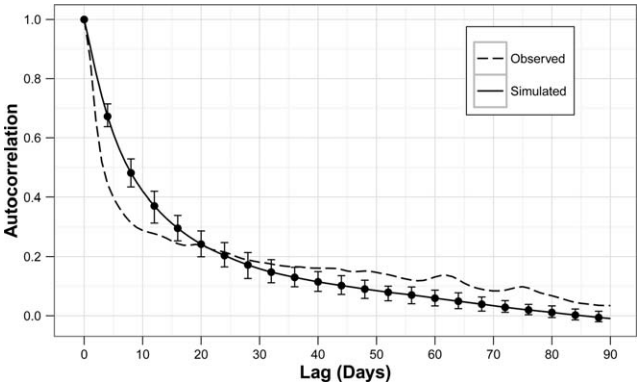

Figure 7. Correlogram of daily streamflow.

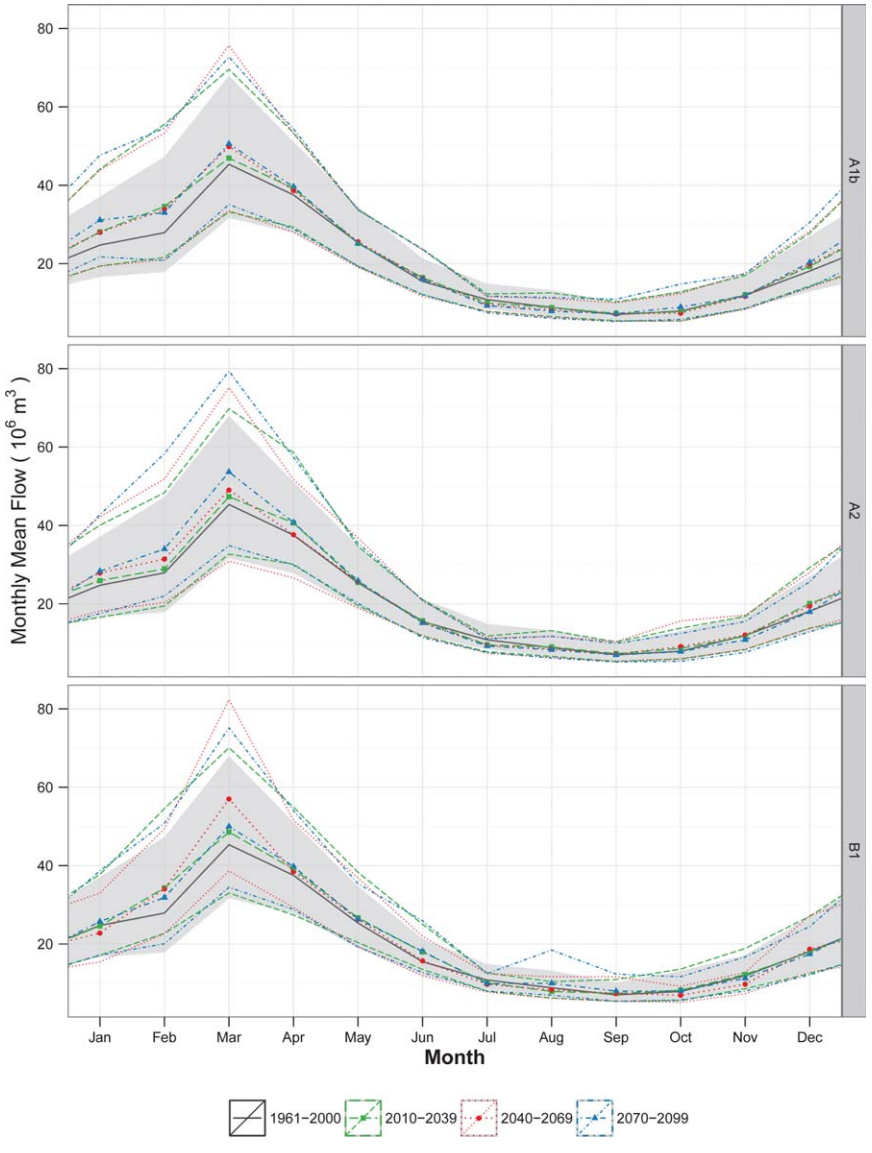

Figure 8. Variation in monthly mean due to climate change (CCC). Median values are displayed as central lines, with black representing the historical record and colored lines representing climate change time steps. The 25th and 75th percentiles are represented by the shaded area for the historical record and thin lines for climate change simulations.

distributions, while the PCM1 model tends to be the "driest" model, producing consistently low daily flow distributions.

[54] Slight seasonal trends exist within the daily flow distributions. Daily flows during the winter months are reproduced well across the entire flow distribution, while the model tends to overpredict low flows during the spring (March and April). Summer flows are captured well, though all GCMs tend to underpredict high (<15% exceedance) flows during the fall, with the remainder of the distribution reproduced very well. Fall storm events may prove difficult to model because they occur during a time period when precipitation events are transitioning from convective to frontal behavior and when hurricanes or tropical storms may impact the region.

[55] The underlying structure of the daily Markov streamflow model adequately reproduces the autocorrelation structure of the daily streamflows (Figure 7), agreeing with similar Markov chain-based streamflow generation models [*Xu et al*., 2001]. Daily streamflow autocorrelation is assumed to be controlled primarily by the model structure, with exponential recession and storm pulses sampled and sorted from the Weibull distribution. Because this example is designed as a case study, the relative influence of the model structure and the potential for higher order Markov chains was not evaluated but could be the subject of further research.

4.7. Predicted Climate Change Effects on Streamflow

[56] The effect of climate change on streamflow in the Potomac River was evaluated by generating daily streamflow time series subject to three climate change emission scenarios (SRES A1b, A2, and B1) for three future time periods (2010–2039, 2040–2069, and 2070–2099).

4.7.1. Annual Flows

[57] Simulation of climate-adjusted streamflows under these emission scenarios suggests an increase in mean annual flow between 1% and 7% by 2070–2099 (Table 5). A consistent increase of 2–4% by 2040–2069 matches closely with *Milly et al*.'s [2005] prediction of a 3.6% increase in mean annual flow. The greatest increase in mean annual flow occurs in the CCC and PCM1 models, while the remaining GCMs show greater variability and only a moderate increase in mean annual flow. In addition to this slight increase in mean annual flow, the CV among annual flows is predicted to increase significantly, suggesting a wider distribution of flows. As expected, these trends continue throughout the century and are most evident for the severe A2 scenario and less detectable for the more moderate B1 scenario.

[58] There is little projected change in the date of the annual maximum flow; however, the date of the minimum annual flow is predicted to occur 2–5 days earlier by the 2070–2099 time period, on average. This shift is consistent across all GCM models and scenarios.

4.7.2. Seasonal Trends

[59] Nearly all GCM simulations show an increase in mean monthly flows for the Potomac River between December and April, with this increase growing throughout the next century (Figure 8). As expected, this increase is greatest for the highest emission scenario, A2. In addition to an increase in the mean winter flows, the distribution of monthly flow is projected to increase in variability, particularly for high flows. This trend of increased flow during the winter and early spring corresponds well with studies by *Najjar et al*. [2009], *Mccabe and Ayers* [1989], and *Hayhoe et al*. [2008], which project similar seasonal shifts.

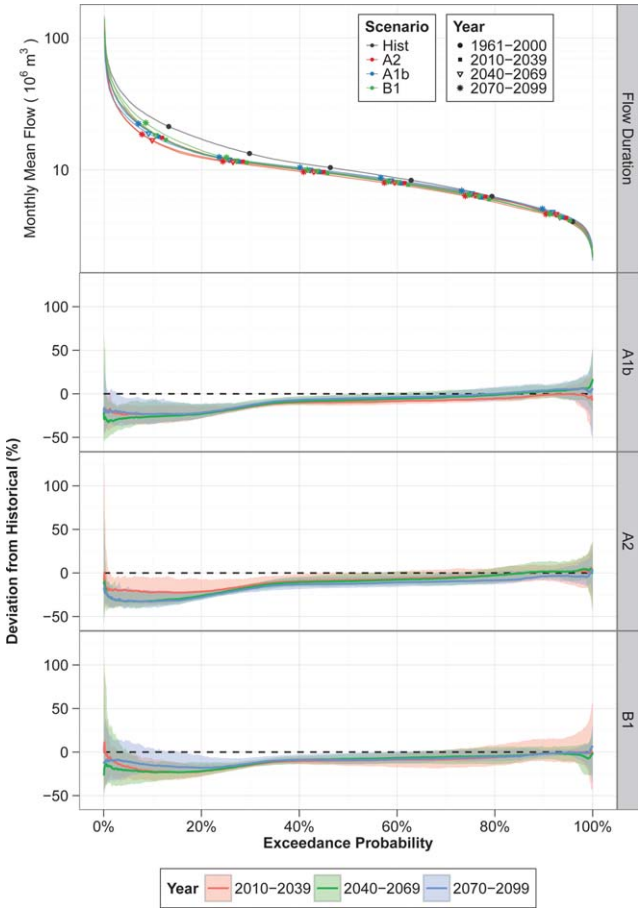

Figure 9. Flow duration curve for July subject to climate change (CCSM). (top) The entire distribution of July flows and (bottom) the percent change relative to the historical.

[60] In contrast, the model realizations predict a decrease in summer flows, particularly for the months of July and August (Figure 8). This seasonal trend is evident for all GCMs except for PCM1.

[61] The months of October and November show the greatest uncertainty in predictions for monthly flows. This is not a surprising result, given the difficulty in modeling these months during validation. The NCAR models (CCSM and PCM1) and CSIRO all predict a significant increase in flow during these months in the future, potentially attributable to tropical storm events or other long duration, high precipitation events, while a similar trend is not evident in other GCM realizations.

4.7.3. Extreme Low Flows

[62] Model estimates of future extreme low flows show a slight decrease in the $7Q_{10}$ minimum flow given the modeled emission scenarios. A notable decrease was detected for all GCMs, except for the NCAR CCSM model, which produces mixed results, and the PCM1 model, which showed a consistent increase. For those models with a decrease in extreme low flows, the $7Q_{10}$ minimum flow is

Table 6. Percent Change in $7Q_{10}$ Minimum Flow for Climate Change Realizations

Model	2010–2039	2040–2069	2070–2099
CCC	−1.82 (−5.98–1.62)	−0.83 (−2.73–0.66)	−0.09 (−3.25 to 4.69)
CCSM	2.21 (1.00–4.57)	−0.03 (−2.07–3.09)	2.60 (−1.66 to 5.84)
CSIRO	−5.74 (−7.87 to −2.09)	−3.11 (−5.63 to −1.34)	−5.57 (−10.06 to −3.32)
MIROC		−1.17 (−2.69 to 0.43)	−4.31 (−5.91 to −1.68)
PCM1	2.99 (2.93–3.05)	3.23 (2.28–4.10)	9.07 (6.94–10.87)

predicted to decrease by 0–10.1%, with the greatest decrease attributable to the A2 emission scenario (Table 6). This trend suggests that droughts will continue to increase in severity over the modeled time period.

4.7.4. Daily Flows

[63] The apparent increase in winter flows is attributable to an increase across the entire streamflow distribution, rather than an increase in a particular range. This trend continues until the transitional months of March and April, where the increase occurs predominantly in the low and middle flows (60–90% exceedance), with little change in extreme low or high flows. The decrease in July and August flow is explained by a consistent decrease across the entire flow distribution, except for extreme low flows (90–99% exceedance) which remain consistent with the historical record (Figure 9).

[64] As in the case of monthly means, the fall months exhibit mixed trends across the projected future climatic conditions. The CCSM, CSIRO, and PCM1 models, which project a significant increase in mean flow during the months of September and October, attribute this to an increase in high streamflow events (exceedance <40%), which further points to an increase in large, sustained rainfall events.

5. Conclusions

[65] A stochastic streamflow method was developed that links a monthly climate model with a daily streamflow generation model. Using discriminant functions, GCM-scale climate data may be related to discrete streamflow states, which in turn control the generation of daily streamflow time series. With engineers and planners increasingly focused on the potential effects of climate change on water resources, this model allows the generation of an infinite set of daily streamflow traces, which can be used for simulation or adaptation studies.

[66] A case study was presented using the Potomac River to evaluate the method. Historical streamflow statistics are reproduced successfully at daily, monthly, and annual time steps, greatly improving on the existing regional HSPF rainfall-runoff model. In addition, daily streamflow dynamics, such as autocorrelation structure, are maintained.

[67] Extending this model to evaluate the effect of climate change on streamflow in the Potomac produced results comparable to other streamflow projections for the Mid-Atlantic. Mean annual streamflow is projected to increase by 1–7% by 2100, with the majority of this increase occurring during the winter and early spring. Conversely, summer flows are projected to decrease, particularly during July and August, caused by a decrease in runoff from large, sustained storm events. This change in summer flow is projected to increase the severity of extreme low flows slightly and to shift the date of the annual minimum flow, which historically occurs in mid-September, 2–5 days earlier by the 2070–2099 time period. The models diverge in their predictions for the fall, suggesting a need for further research and potentially additional climate predictors. Some GCMs predict a large increase in monthly mean flows during September and October, which may point to an increase in tropical storm events.

[68] The included case study presents the streamflow analysis and simulation process as applied to an individual streamflow station; however, this model may be expanded to simulate climate-adjusted streamflow at multiple locations within a watershed using spatial disaggregation techniques such as the method of fragments [*Porter and Pink*, 1991] or by simulating at each location simultaneously using a covariate term. The proposed method offers an alternative to rainfall-runoff modeling for generating climate-adjusted streamflow time series. This method is not universally applicable. In particular, it does not provide detailed, physical output on water balance within the watershed and assumes a stationary hydrologic system (i.e., no land-cover changes). However, for the purposes of generating long series of realistic current and climate-adjusted streamflow, the method has great utility and should be expanded with additional research. Future studies may test the models applicability in a wider range of climates, expand the set of climate predictors to include atmospheric circulation or periodic indices (ENSO), and evaluate the use of Bayesian approaches to defining the parameter values in the streamflow generation model.

[69] **Acknowledgments.** James Stagge is a Via Doctoral Fellow and gratefully acknowledges support from the Charles E. Via, Jr. Scholars Program and the Institute for Critical Technology and Applied Science (ICTAS). The authors would also like to thank the Interstate Commission on the Potomac River Basin (ICPRB) and Hydrologics, Inc. for providing data access and research support.

References

Ahmed, S. N., K. R. Bencala, and C. L. Schultz (2010), Washington Metropolitan Area water supply reliability study, Part 1: Demand and resource availability forecast for the year 2040, *Tech. Rep. ICPRB 10-01*, Interstate Comm. on the Potomac River Basin, Rockville, Md.

Aksoy, H. (2003), Markov chain-based modeling techniques for stochastic generation of daily intermittent streamflows, *Adv. Water Resour.*, *26*(6), 663–671.

Aksoy, H., and M. Bayazit (2000), A model for daily flows of intermittent streams, *Hydrol. Processes*, *14*(10), 614–633.

Bardossy, A., and E. J. Plate (1992), Space-time model for daily rainfall using atmospheric circulation patterns, *Water Resour. Res.*, *28*(5), 1247–1259.

Bartolini, P., and J. D. Salas (1993), Modeling of streamflow processes at different time scales, *Water Resour. Res.*, *29*(8), 2573–2587.

Beard, L. R. (1967), Simulation of daily streamflows, paper presented at International Hydrology Symposium, ASCE, Fort Collins, Colo.

Bellone, E., J. P. Hughes, and P. Guttrop (2000), A hidden Markov model for downscaling synoptic atmospheric patterns to precipitation amounts, *Clim. Res.*, *15*, 1–12.

Box, G., and G. M. Jenkins (Eds.) (1970), *Time Series Analysis, Forecasting and Control*, Holden-Day, San Francisco, Calif.

Box, G. E. P., and D. R. Cox (1964), An analysis of transformations, *J. R. Stat. Soc., Ser. B*, *2*, 211–252.

Buishand, T. A., and T. Brandsma (2001), Multisite simulation of daily precipitation and temperature in the Rhine basin by nearest-neighbor resampling, *Water Resour. Res.*, *37*, 2761–2776.

Cattell, R. B. (1966), The scree test for the number of factors, *Multivar. Behav. Res.*, *1*(2), 245–276.

Chapman, T. (1997), Stochastic modelling of daily rainfall in the Western Pacific, *Math. Comput. Simulat.*, *43*, 351–358.

Collins, W. D., et al. (2006), The Community Climate System Model Version 3 (CCSM3), *J. Clim.*, *19*, 2122–2143.

Compo, G. P., et al. (2011), The Twentieth Century Reanalysis Project, *Q. J. R. Meteorol. Soc.*, *137*(654), 1–28.

Corte-Real, J., B. Quian, and H. Xu (1999), Circulation patterns, daily precipitation in Portugal and implications for climate change simulated by the second Hadley Centre GCM, *Clim. Dyn.*, *15*, 921–935, doi:10.1007/s003820050322.

Dai, A. (2006), Precipitation characteristics in eighteen coupled climate models, *J. Clim.*, *19*(18), 4605–4630.

Delignette-Muller, M. L., R. Pouillot, J.-B. Denis, and C. Dutang (2010), *fitdistrplus: Help to Fit of a Parametric Distribution to Non-Censored or Censored Data*, r package version 0.1–3.

Eden, J. M., M. Widmann, D. Grawe, and S. Rast (2012), Skill, correction, and downscaling of GCM-simulated precipitation, *J. Clim.*, *25*(11), 3970–3984.

Flato, G. (2005), The Third Generation Coupled Global Climate Model (CGCM3), http://www.cccma.bc.ec.gc.ca/models/cgcm3.shtml.

Gordon, H. B., et al. (2002), The CSIRO Mk3 climate system model, *Tech. Rep. 60*, CSIRO Atmos. Res. Tech. Pap, Melbourne, Australia.

Groisman, P. Y., R. W. Knight, and T. R. Karl (2001), Heavy precipitation and high streamflow in the contiguous United States: Trends in the twentieth century, *Bull. Am. Meteorol. Soc.*, *82*(2), 219–246.

Groisman, P. Y., R. W. Knight, T. R. Karl, D. R. Easterling, B. Sun, and J. H. Lawrimore (2004), Contemporary changes of the hydrological cycle over the contiguous United States: Trends derived from in situ observations, *J. Hydrometeorol.*, *5*(1), 64–85.

Grygier, J. C., and J. R. Stedinger (1988), Condensed disaggregation procedures and conservation corrections for stochastic hydrology, *Water Resour. Res.*, *24*(10), 1574–1584.

Guttman, L. (1954), Some necessary conditions for factor analysis, *Psychometrika*, *19*, 149–161.

Harms, A. G., and T. H. Campbell (1967), An extension to the Thomas-Fiering model for the sequential generation of streamflow, *Water Resour. Res.*, *3*(3), 653–661.

Hayhoe, K., et al. (2008), Regional climate change projections for the Northeast USA, *Mitigat. Adapt. Strat.Global Change*, *13*, 425–436.

Hirsch, R. (1979), Synthetic hydrology and water supply reliability, *Water Resour. Res.*, *15*(4), 1603–1615, doi:10.1029/WR015i006p01603.

Horn, J. L. (1965), A rationale and test for the number of factors in factor analysis, *Psychometrika*, *30*(2), 179–185.

Hotelling, H. (1933), Analysis of a complex of statistical variables into principal components, *J. Educ. Psychol.*, *24*(6), 417–441.

Hughes, J. P., and P. Guttorp (1994), A class of stochastic models for relating synoptic atmospheric patterns to regional hydrologic phenomena, *Water Resour. Res.*, *30*, 1535–1546, doi:10.1029/93WR02983.

Huth, R. (1999), Statistical downscaling in central Europe: Evaluation of methods and potential predictors, *Clim. Res.*, *13*, 91–101.

Kaiser, H. F. (1960), The application of electronic computers to factor analysis, *Educ. Psychol. Meas.*, *20*(1), 141–151.

Kalkstein, L. S., G. Tan, and J. A. Skindlov (1987), An evaluation of three clustering procedures for use in synoptic climatological classification, *J. Appl. Meteorol.*, *26*, 717–730, doi:10.1175/1520-0450(1987)026<0717:AEOTCP>2.0.CO;2.

Kottegoda, N. T. (1980), *Stochastic Water Resources Technology*, John Wiley, New York.

Lall, U., and A. Sharma (1996), A nearest neighbor bootstrap for resampling hydrologic time series, *Water Resour. Res.*, *32*(3), 679–693.

Lau, K. M., Y. Sud, and J. H. Kim (1996), Intercomparison of hydrologic processes in AMIP GCMs, *Bull. Am. Meteorol. Soc.*, *77*(10), 2209–2227.

Maheepala, S., and B. J. C. Perera (1996), Monthly hydrologic data generation by disaggregation, *J. Hydrol.*, *178*(1–4), 277–291.

Matalas, N. C. (1997), Stochastic hydrology in the context of climate change, *Clim. Change*, *37*, 89–101.

Maurer, E. P., and H. G. Hidalgo (2008), Utility of daily vs. monthly large-scale climate data: An intercomparison of two statistical downscaling methods, *Hydrol. Earth Syst. Sci.*, *12*(2), 551–563.

Mccabe, G. J., Jr., and M. A. Ayers (1989), Hydrologic effects of climate change in the Delaware River basin, *Water Resour. Bull.*, *25*, 1231–1242.

Mearns, L. O., F. Giorgi, L. McDaniel, and C. Shields (1995), Analysis of daily variability of precipitation in a nested regional climate model: Comparison with observations and doubled CO2 results, *Global Planet. Change*, *10*(1–4), 55–78.

Meehl, G. A., C. Covey, T. Delworth, M. Latif, B. McAvaney, J. F. B. Mitchell, R. J. Stouffer, and K. E. Taylor (2007a), The WCRP CMIP3 multi-model dataset: A new era in climate change research, *Bull. Am. Meteorol. Soc.*, *88*, 1383–1394.

Meehl, G. A., et al. (2007b), Global climate projections, in *Climate Change 2007: The Physical Science Basis. Working Group I Contribution to the Fourth Assessment Report of the Intergovernmental Panel on Climate Change*, chap. 10, pp. 747–845, Cambridge Univ. Press, New York.

Michelangeli, P. A., R. Vautard, and B. Legras (1995), Weather regimes: Recurrence and quasi stationarity, *J. Atmos. Sci.*, *52*, 1237–1256, doi:10.1175/1520-0469(1995)052<1237:WRRAQS>2.0.CO;2.

Milly, P. C. D., K. A. Dunne, and A. V. Vecchia (2005), Global pattern of trends in streamflow and water availability in a changing climate, *Nature*, *438*(7066), 347–350.

Moore, M. V., et al. (1997), Potential effects of climate change on freshwater ecosystems of the New England/Mid-Atlantic region, *Hydrol. Processes*, *11*(8), 925–947.

Najjar, R., L. Patterson, and S. Graham (2009), Climate simulations of major estuarine watersheds in the Mid-Atlantic region of the US, *Clim. Change*, *95*, 139–168.

Payne, K., W. R. Neumann, and K. D. Kerri (1969), Daily streamflow simulation, *J. Hydraul. Div. Proc. Am. Soc. Civ. Eng.*, *95*, 1163–1179.

Porter, J. W., and B. J. Pink (1991), A method of synthetic fragments for disaggregation in stochastic data generation, paper presented at International Hydrology and Water Resources Symposium, Inst. of Eng., Canberra, Australia.

Prairie, J. R., B. Rajagopalan, T. J. Fulp, and E. A. Zagona (2006), Modified K-NN model for stochastic streamflow simulation, *J. Hydrol. Eng.*, *11*(4), 371–378.

Pyke, C. R., et al. (2008), Climate change and the Chesapeake Bay: State-of-the-science review and recommendations, *Order J. Theory Ordered Sets Appl.*, *7415*(9), 1–6.

Quimpo, R. G. (1968), Stochastic analysis of daily river flows, *J. Hydraul. Div. Proc. Am. Soc. Civ. Eng.*, *94*, 43–57.

Quimpo, R. G., and V. Yevjevich (1967), Stochastic description of daily river flows, paper presented at the International Hydrology Symposium, ASCE, Fort Collins, Colo.

Sansom, J., and P. Thomson (2007), On rainfall seasonality using a hidden semi-Markov model, *J. Geophys. Res.*, *112*, D15105, doi:10.1029/2006JD008342.

Sargent, D. M. (1979), A simplified model for the generation of daily streamflows, *Hydrol. Sci. J.*, *24*(4), 509–527.

Sharma, A., D. G. Tarboton, and U. Lall (1997), Streamflow simulation: A nonparametric approach, *Water Resour. Res.*, *33*(2), 291–308.

Srikanthan, R., and T. McMahon (2001), Stochastic generation of annual, monthly and daily climate data: A review, *Hydrol. Earth Syst. Sci.*, *5*(4), 653–670.

Srikanthan, R., and T. A. McMahon (1982), Stochastic generation of monthly streamflows, *J. Hydraul. Div. ASCE*, *108*(3), 419–441.

Stagge, J. H., and G. E. Moglen (2011), Regional effects of land use change on water supply in the Potomac river basin, *Watershed Sci. Bull.*, *2*(2), 52–53.

Stedinger, J. R., and R. M. Vogel (1984), Disaggregation procedures for generating serially correlated flow vectors, *Water Resour. Res.*, *20*(1), 47–56.

Stedinger, J. R., D. P. Lettenmaier, and R. M. Vogel (1985), Multisite ARMA (1, 1) and disaggregation models for annual streamflow generation, *Water Resour. Res.*, *21*(4), 497–509.

Szilagyi, J., G. Balint, and A. Csik (2006), Hybrid, Markov chain-based model for daily streamflow generation at multiple catchment sites, *J. Hydrol. Eng.*, *11*(3), 245–256.

Tabachnick, B. G., and L. S. Fidell (2007), Using Multivariate Statistics, *5th ed.*, Allyn and Bacon, Boston, Mass.

Tallaksen, L. (1995), A review of baseflow recession analysis, *J. Hydrol.*, *165*(3), 349–370.

Tebaldi, C., K. Hayhoe, J. M. Arblaster, and G. A. Meehl (2006), Going to the extremes, *Clim. Change*, *79*(3–4), 185–211.

Thomas, H. A., and M. B. Fiering (1962), Mathematical synthesis of stream flow sequences for the analysis of river basins by simulation, in *Design of Water Resources*, edited by A. Maass et al., Harvard Univ. Press, Cambridge, Mass.

Thyer, M., and G. Kuczera (2003), A hidden Markov model for modelling long-term persistence in multi-site rainfall time series 1: Model calibration using a Bayesian approach, *J. Hydrol.*, *275*, 12–26.

Treiber, B., and E. J. Plate (1975), A stochastic model for the simulation of daily flows, paper presented at International Symposium and Workshops on the Application of Mathematical Models in Hydrology and Water Resource Systems, Bratislava, Slovakia.

U.S. Environmental Protection Agency (2010), Chesapeake Bay Phase 5.3 Community Watershed Model, EPA 903S10002 - CBP/TRS-303-10, U.S. Environ. Prot. Agency, Chesapeake Bay Prog. Off., Annapolis, Md.

Valencia, R. D., and J. C. Schakke Jr. (1973), Disaggregation processes in stochastic hydrology, *Water Resour. Res.*, *9*(3), 580–585, doi:10.1029/WR009i003p00580.

Vogel, R. M., and A. L. Shallcross (1996), The moving blocks bootstrap versus parametric time series models, *Water Resour. Res.*, *32*(6), 1875–1882.

Ward, J. H. (1963), Hierarchical grouping to optimize an objective function, *J. Am. Stat. Assoc.*, *58*(301), 236–244.

Washington, W. M., et al. (2000), Parallel climate model (PCM) control and transient simulations, *Clim. Dyn.*, *16*, 755–774.

Watanabe, S., et al. (2011), MIROC-ESM: Model description and basic results of CMIP5–20c3m experiments, *Geosci. Model Dev. Discuss.*, *4*, 1063–1128.

Weiss, G. (1977), Shot noise models for the generation of synthetic streamflow data, *Water Resour. Res.*, *13*(1), 101–108.

Widmann, M., and C. S. Bretherton (2000), Validation of mesoscale precipitation in the NCEP reanalysis using a new gridcell dataset for the northwestern United States, *J. Clim.*, *13*(11), 1936–1950.

Widmann, M., C. S. Bretherton, and E. P. Salathé (2003), Downscaling over the northwestern United States using numerically simulated precipitation as a predictor, *J. Clim.*, *16*(5), 799–816.

Wilby, R.L., and T. M. L. Wigley (2000), Precipitation predictors for downscaling: Observed and general circulation model relationships, *Int. J. Climatol.*, *20*(6), 641–661.

Xu, Z. X., A. Schumann, and C. Brass (2001), Markov autocorrelation pulse model for two sites daily streamflow, *J. Hydrol. Eng.*, *6*, 189–195.

Yarnal, B., and J. D. Draves (1993), A synoptic climatology of stream flow and acidity, *Clim. Res.*, *2*, 193–202.